JACS
JOURNAL OF THE AMERICAN CHEMICAL SOCIETY

Article

pubs.acs.org/JACS

Base-Excision Repair Activity of Uracil-DNA Glycosylase Monitored Using the Latch Zone of α-Hemolysin

Qian Jin, Aaron M. Fleming, Robert P. Johnson, Yun Ding, Cynthia J. Burrows,* and Henry S. White*

Department of Chemistry, University of Utah, 315 South 1400 East, Salt City, Utah 84112-0850, United States

Supporting Information

ABSTRACT: Nanopores have been investigated as a simple and label-free tool to characterize DNA nucleotides when a ssDNA strand translocates through the constriction of the pore. Here, a wild-type α-hemolysin protein nanopore was used to monitor DNA repair enzyme activity based on base-specific interactions of dsDNA with the vestibule constriction "latch", a previously unrecognized sensing zone in α-hemolysin specific for dsDNA structure. The presence of a single abasic site within dsDNA that is in proximity to the latch zone (±2 nucleotides) results in a large increase in ion channel current, allowing accurate quantitation of the kinetics of base repair reactions involving an abasic site product. Taking advantage of the high resolution for abasic site recognition, the rate of uracil-DNA glycosylase hydrolysis of the N-glycosidic bond, converting 2′-deoxyuridine in DNA to an abasic site, was continuously monitored by electrophoretically capturing reaction substrate or product dsDNA in the ion channel vestibule. Our work suggests use of the nanopore as an enzymology tool and provides a means to identify single base structural changes in dsDNA.

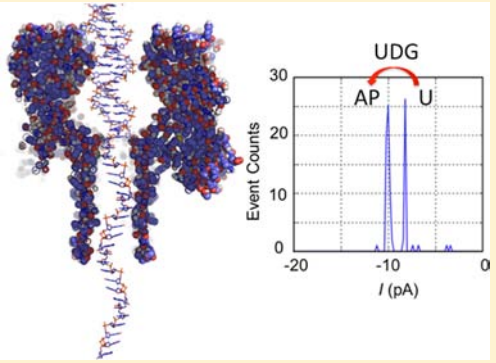

INTRODUCTION

Deamination of cytosine to yield uracil (U) leads to a U:G (guanine) mismatch that is one of the most common forms of DNA hydrolytic damage,[1] occurring at a rate of 100−500 times per cell per day.[2] Left unrepaired, the U:G base pair causes a T:A (thymine: adenine) mutation upon replication, disturbing genome integrity.[3] In addition, the coding of the resulting mutation into mRNA may give rise to translational errors during protein expression.[4] To repair the deamination lesions, the DNA repair enzyme uracil-DNA glycosylase (UDG) initiates the base excision repair (BER) pathway by cleaving the N-glycosidic bond between the uracil base and the sugar of the nucleotide, leaving an abasic site (AP, Figure 1).[5−7] The BER pathway is completed by the coordinated work of additional enzymes that act to remove the abasic site from the duplex and replace it with the correct cytosine base.[8]

The commonly used approach to measure UDG activity involves quenching aliquots of the reaction solution at a series of time intervals followed by gel electrophoresis.[9−13] This method is complicated by the procedure of radioactive or fluorescent labeling as well as the long gel development time.[14] Here, we demonstrate a label-free and time-efficient method to monitor UDG activity using nanopore ion-channel recordings. The protein nanopore α-hemolysin (α-HL) has been widely studied as a stochastic detector for structural discrimination at the single-molecule level.[15−20] The interactions of α-HL with synthetic polymers, RNA, DNA and proteins provide valuable information to characterize conformations and biophysical properties (including inter- and intramolecular interactions) of these molecules.[21−27] In nanopore-based DNA analysis, DNA is driven by the electrophoretic force into the vestibule of α-HL, causing a temporal blockage to the ion flux through the channel.[28,29] While single-stranded DNA can translocate through α-HL, the diameter of dsDNA (2.0 nm) is larger than the narrowest constriction of the protein channel (1.4 nm). Thus, DNA duplex structures are required to "unzip" in

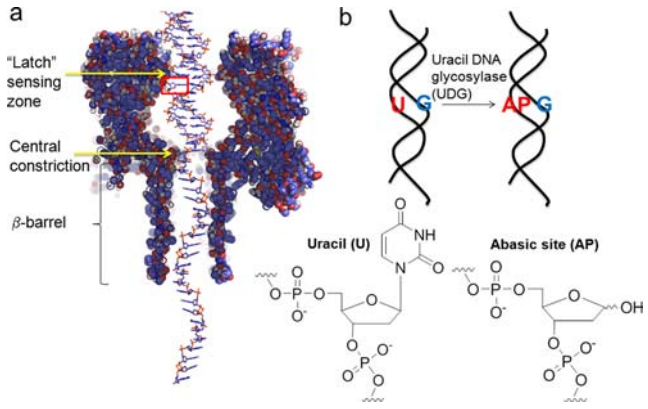

Figure 1. Monitoring the UDG enzyme activity for dsDNA using a WT α-HL channel. (a) The structure of dsDNA with a 5′-poly(T)$_{24}$ tail within WT α-HL. The box indicates the location of the uracil (U) base or the abasic site (AP). (b) Scheme of the UDG hydrolysis reaction. The α-HL structure was taken from pdb 7AHL.[38] DNA structure is shown on a 1:1 scale with α-HL.

Received: October 16, 2013
Published: December 2, 2013

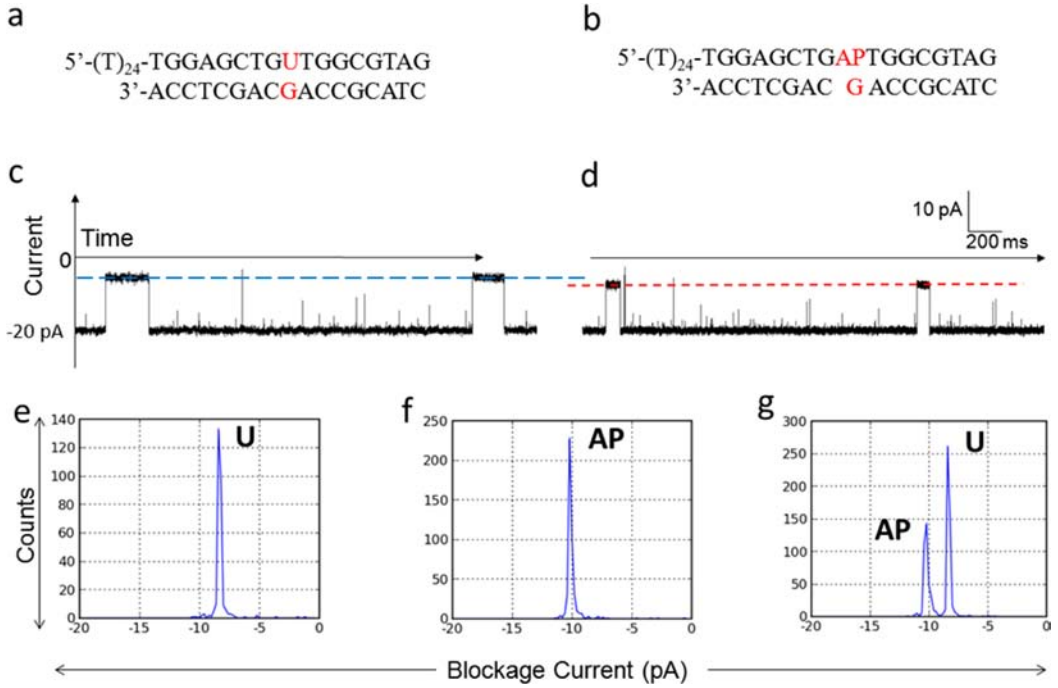

Figure 2. Single-nucleotide recognition was achieved between the U-containing duplex (a, c, and e) and the AP-containing duplex (b, d, and f) based on a ~2 pA difference in blockage current levels of the unzipping events in a 14 μM DNA, 150 mM buffered KCl solution at −120 mV (*cis* vs *trans*). (a) Sequence of the starting material formed by a 41-mer U-containing strand hybridized to a 17-mer strand. (b) Sequence of the product containing AP. (c,d) Sample current−time (i−t) traces for blockages generated by the U duplex (c) or the AP duplex (d) in individual experiments. The blue and red lines indicate the current blockage levels used to determine the duplex identity. Examples of longer (20 s) i−t traces for the U and AP duplexes are presented in the Supporting Information. (e,f,g) Histograms of current blockage levels for the U duplex (e), AP duplex (f), and a mixture of U and AP duplexes (g, mole ratio ~2:1).

order for the separated oligomers to translocate through the nanopore.[30−32] DNA duplex events are characterized by both the degree to which the duplex blocks the flux of electrolyte ions (K^+ and Cl^-) and the time duration while the duplex sits in the protein vestibule prior to unzipping.[33]

In the present report, UDG conversion of a U-containing duplex to an AP-containing duplex was continuously monitored by capture of the duplexes in an α-HL channel (Figure 1). The difference in current blockages of the U- and AP-containing duplexes during unzipping was used to determine, on a single-molecule basis with high accuracy, the presence of U or AP structures. The quantitative conversion of the U- to AP-duplex studied by single-molecule events of duplex unzipping was used to extract kinetic information for the UDG digestion reaction. Previous nanopore-based studies of DNA enzyme kinetics have focused on the activity of a DNA polymerase, an enzyme that can slow down the DNA translocation speed through α-HL, and thus is potentially useful in sequencing.[34−37] RNA ribonuclease activity has also been studied using nanopores, generating an increased event rate after ribonuclease cleaves RNA into fragments.[15]

The location of U or AP within the duplex investigated is in the vicinity of the vestibule constriction, or the "latch" region as defined by Song et al.,[38] assuming each nucleotide is 0.34 nm long, and the duplex with a 5′-poly$(T)_{24}$ tail is driven by the electric field tail first into the central constriction of α-HL (Figure 1a). Intensive investigations of DNA in WT α-HL, as well as efforts to engineer α-HL aimed at improving sensitivity, have focused on ssDNA structural analysis in the sensing zone defined by the 1.4-nm-diameter central constriction and the β-barrel section of the channel.[39−43] The ability to distinguish an abasic site in a DNA duplex far from the narrowest constriction of α-HL indicates the presence of a well-defined, previously unrecognized sensing zone specific to dsDNA in the WT α-HL channel. We capitalize on this new discovery to monitor the kinetics of the UDG base excision repair reaction.

RESULTS AND DISCUSSION

A U:G base pair was embedded into a 17-bp heterosequence duplex as the starting material of the UDG reaction (Figure 2a). A poly$(T)_{24}$ tail was included at the 5′-end of the U-containing strand to facilitate threading into the α-HL ion channel. Voltage-driven unzipping of DNA duplexes was initiated by pulling the 5′-tail of the molecule into the α-HL channel. Our previous work reported distinct current levels in 1 M KCl due to 3′ and 5′ entry if the duplex has two single-stranded tails.[44] Thus, the 3′-end was left blunt to avoid complication of different blockage currents that originate from the directionality effect of entry. The blunt end of the duplex does not enter into the vestibule in 150 mM KCl (SI Figure 1), in agreement with a previous observation.[15] The electrical signature of the unzipping duplex was used to determine the identity of the duplex containing either U or an AP site.

A 150 mM KCl, 20 mM Tris·HCl, 1 mM EDTA, pH = 7.7 solution was used as the electrolyte for nanopore ion-channel recordings. Because the catalytic activity of UDG is disrupted by electrostatic interaction between the enzyme and DNA substrate at high ionic strength (>200 mM), 150 mM KCl was selected as the electrolyte concentration,[45,46] significantly lower than KCl concentrations of ~1 M used in the majority of previous α-HL ion channel studies. The lower electrolyte concentration results in fewer duplex capture events relative to

dx.doi.org/10.1021/ja410615d | J. Am. Chem. Soc. 2013, 135, 19347−19353

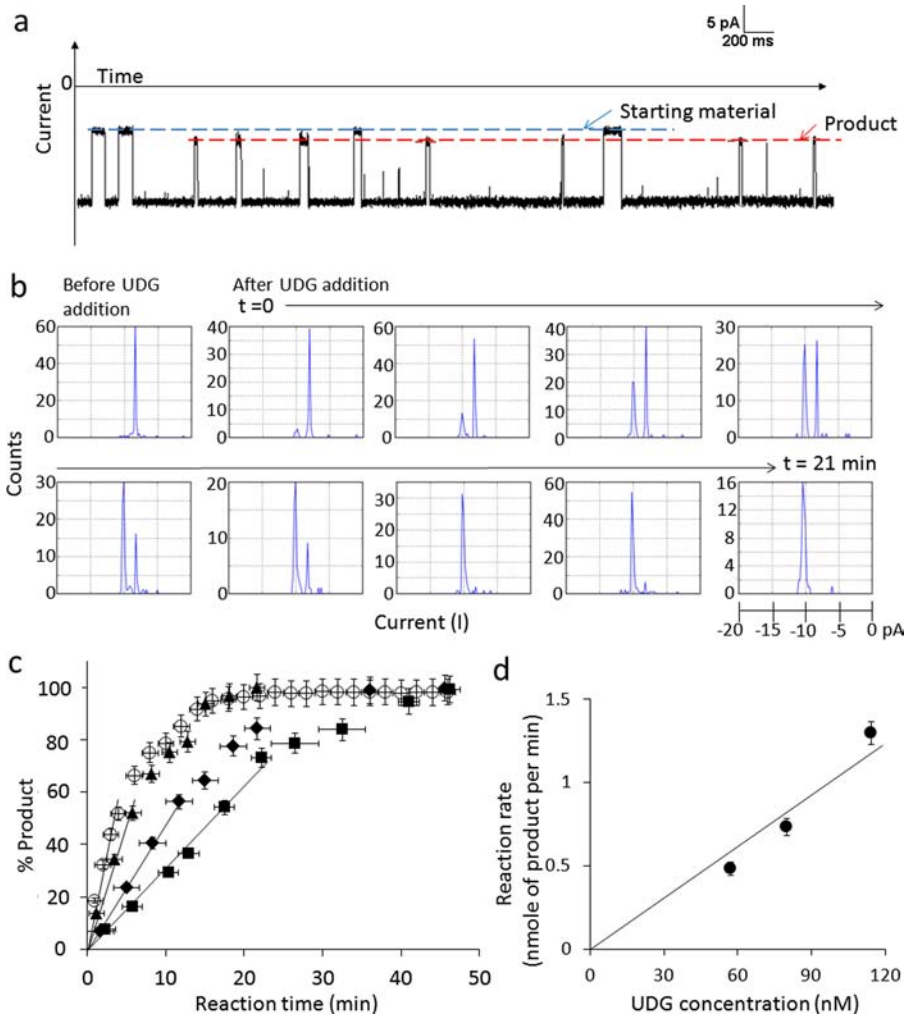

Figure 3. Monitoring the UDG reaction using a nanopore. (a) A representative 5-s-long $i-t$ trace collected ~7 min after UDG addition to the solution containing the substrate DNA (Figure 3a). The 350 μL solution contained 43 μM DNA and 110 nM UDG in the 350 μL reaction chamber. The two current blockage levels (blue and red dashed lines) correspond to the substrate (U) and product (AP), respectively. (b) Time-dependent histograms of blockage currents correspond to the progression of the enzymatic reaction. Each histogram after UDG addition includes unzipping events that occur within a 140 s interval. The time that UDG was added to the solution was set at t = 0. (c) Enzyme kinetic curves obtained from nanopore experiments using 43 μM U-containing duplexes treated with 57 (squares), 80 (diamonds), and 110 (triangles) nM UDG. The x-axis bars correspond to the time window used to obtain each histogram (see SI Figures 9 and 10). The ±5% errors on the y-axis were estimated from a repeated measurement (see Supporting Information). Gel electrophoresis profiling was performed on the enzyme reaction of 43 μM U-containing duplexes treated with 110 nM of UDG in 150 mM KCl buffered solution at 22 °C, the results of which are plotted as open circles. Black lines correspond to a linear fit during the burst phase. (d) Enzymatic reaction rates measured by nanopore experiments are computed from the slope of the black lines in (c) are plotted as a function the UDG amount. The error bars are from the linear fits to the data in (c).

1 M KCl solutions; typically, we observed capture rates of 0.1 to 0.5/s at ~10 μM dsDNA, at an applied transmembrane potential of −120 mV (*cis* vs *trans*).

The ability of WT α-HL to yield single-nucleotide discrimination between U and AP was examined by performing nanopore unzipping experiments at 22 °C. The U-containing duplex and the AP-containing duplex (Figure 2a and b) at a concentration of 14 μM were added, in separate experiments, to the 350 μL volume in the *cis* reservoir. Both duplexes generated a uniform level of current blockage during unzipping, with the U-containing duplex blocking the channel ~2 pA more than the AP-containing one (Figure 2c and d). Histograms of the current blockage levels for individual U- and AP-containing duplexes display very narrow distributions (Figure 2e and f); analogous experiments in which both duplexes were present in solution yield baseline resolved current histograms (Figure 2g), demonstrating that the fractional content of each duplex captured from the bulk solution can be quantitatively measured with an essentially immeasurably small error (equivalent to molecular recognition at the single-event level). The unzipping time durations for the U- and AP-containing duplexes partially overlap, and each displays first-order exponential kinetics with reaction time constants of 110 ± 20 ms and 14 ± 2 ms, respectively (SI Figure 2).

Next, the U-containing duplex (43 μM) was treated with UDG (110 nM) directly in the nanopore solution reservoir, coated in a prior step with bovine serum albumin (BSA) to prevent UDG from adsorbing to the polycarbonate reservoir surface. The UDG-catalyzed conversion of the U- to AP-containing duplex was monitored by recording single-molecule unzipping events in the nanopore at −120 mV (*cis* vs *trans*), 22 °C in 150 mM KCl buffered solution (Figure 3). Prior to UDG

dx.doi.org/10.1021/ja410615d | J. Am. Chem. Soc. 2013, 135, 19347−19353

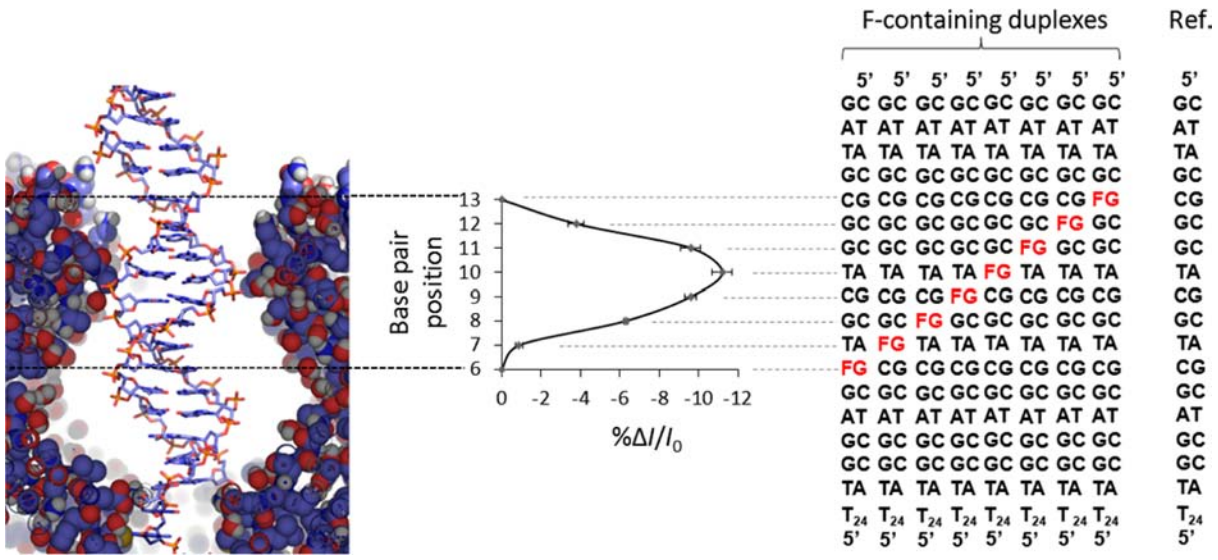

Figure 4. Mapping the resolution of the latch sensing zone of α-HL for dsDNA duplex. (Left) Structures of the inner space of the α-HL vestibule and dsDNA residing within it. (Right) A series of duplexes with a F:G base pair placed at positions 6−13 were examined in the nanopore experiments (150 mM KCl buffered solution, −120 mV). Positions are numbered relative to the 3′-end of the shorter strand. Residual currents ($\%\Delta I/I_0$) measured during unzipping are plotted relative to the reference complementary duplex. The positions 7−12 duplexes generated shallower blockages than the reference, corresponding to negative values of $\%\Delta I/I_0$. The positions 6 and 13 duplexes blocked the channel to the same degree as the reference, corresponding to a zero $\%\Delta I/I_0$. The y-axis positional data are placed at their corresponding locations in the α-HL. The error bars are based on standard deviations of the mean in current blockage histograms, details of which are given in Supporting Information.

addition, a single blockage level was observed (Figure 3b top left histogram), corresponding to the U-containing duplex. After addition of UDG, a second current blockage level corresponding to the AP-containing duplex was detected, indicating the enzymatic conversion of U to AP. The identity of the duplex was determined by examining the current amplitude of the unzipping events, with −8.3 ± 0.2 pA being attributed to the starting material and −10.2 ± 0.2 pA to the product, consistent with the results of control experiments shown in Figure 2. The progress of the reaction was monitored through time-dependent histograms of blockage currents (Figure 3b), in which the relative peak heights for the two species varied and transitioned from the U to AP current levels.

Enzyme kinetic results obtained from nanopore experiments are plotted as the percentage of the AP-containing duplex versus reaction time and are compared with those from gel electrophoresis using the same reaction conditions (Figure 3c). These enzyme kinetic curves demonstrate that UDG hydrolyzes the *N*-glycosidic bond at a nearly linear rate at the beginning of the reaction, and slows down as the reaction reaches completion. The reaction rate of UDG hydrolysis in the nanopore experiment, obtained from the linear slope of the beginning of enzyme kinetic curve, was found to be in good agreement with the value from gel electrophoresis, 1.6 ± 0.4 (2σ) and 1.3 ± 0.2 nmol/min, respectively. In separate experiments (Figure 3c), the same amount of DNA substrate (43 μM) was treated with solutions containing 57 and 80 nM UDG. A linear dependence of reaction rate on UDG concentration, Figure 3d, indicates that the enzyme is the rate-limiting element of the reaction, as anticipated based on the large excess of DNA substrate.

The open channel current for WT α-HL is ∼−20 pA in a 150 mM KCl buffered solution at 120 mV; thus, the ∼2 pA difference generated by substituting U with AP corresponds to a ∼10% difference in residual current. This remarkable single-nucleotide discrimination corresponds to unlabeled DNA duplexes, in contrast the development of more elaborate methods to increase the resolution of discriminating nucleotides in ssDNA (by 2.5% to 8%) using engineered pores or modified DNA bases.[47,48]

Noticing that the uracil base is located in a duplex context at the latch of α-HL, we suggest that the latch region of α-HL constitutes a sensitive zone for structural analysis in dsDNA. Ion channel recordings of a series of duplexes each containing a single tetrahydrofuran (THF or F), a stable analogue of an AP site, at different positions in the duplex sequence were performed in order to determine the sensitivity of residual current as a function of the base position (Figure 4). Current blockage levels for F-containing duplexes were indistinguishable from AP-containing duplexes (SI Figure 3). A set of duplexes with F at positions 6 to 13 relative to the 3′-end of the shorter strand were studied, covering a range of positions around the latch, with position 6 located in the wider space deep in the vestibule, position 13 out of the vestibule, and position 10 approximately at the narrowest constriction of the vestibule. Residual currents ($\%\Delta I/I_0$), corresponding to the percentage of blockage current relative to the reference duplex, and normalized by the open channel current, are plotted in Figure 4. A complementary duplex (sequence shown in Figure 4) was chosen as the reference to set the baseline of $\%\Delta I/I_0$ (SI Figure 8); the current blockage level of the reference duplex was arbitrarily assigned as 0.

A maximum in absolute value of $\%\Delta I/I_0$ occurs when F is placed at position 10, supporting our hypothesis of a sensing zone for duplexes within the latch region. The width of the plot of $\%\Delta I/I_0$ as a function of nucleotide position is approximately ±2 nucleotides from the latch. $\%\Delta I/I_0$ values measured for the same set of duplexes with F at positions 6 to 13 but at different KCl concentrations (up to 1 M) displayed a similar magnitude, with a maximum at position 10 and a similar sensing zone width.

dx.doi.org/10.1021/ja410615d | J. Am. Chem. Soc. 2013, 135, 19347−19353

Additional experiments were conducted to examine the effect of moving F outside of the sensing zone defined by the data in Figure 4 (see Supporting Information). When F was moved to position 5 we observed that the blockade events were characterized by very short unzipping times (<5 ms) and a very broad distribution of blockage currents. When F was placed at position 14, the current was blocked to a lesser degree (by ∼1 pA) than at position 13. Neither of these results follows the trend shown in Figure 4. We hypothesize that the proximity of F near the ends of the duplex can cause fraying, leading to these different behaviors. We are currently investigating the dependence of the blockage current on the length of the duplex extending out of the vestibule and this study will be reported elsewhere. In spite of the rich complexity of the dependencies of the current on the position of the base modification, the data in Figure 4 clearly demonstrate that the latch region can discriminate single base modifications in duplex dsDNA.

The similarity of the dsDNA cross section (2 nm) and the latch diameter (2.6 nm) suggests that the current blockage may be dominated by the duplex filling the volume in the latch region, thereby constricting the ion flux in that region.[38] The shallower blockage when F is in close proximity to the latch can be attributed to the absence of a base in dsDNA within the vestibule constriction. A shallower blockage was also observed when F was placed in ssDNA within the well-studied β-barrel.[49] Our discovery of the sensing capability of the latch region appears consistent with a previous study in which DNA hairpins containing a loop too large to enter the vestibule, but having different stem lengths that entered into the latch region to different degrees, were differentiated based on blockage currents.[50]

Other factors besides size exclusion may need to be considered to explain the nucleotide resolution observed in the latch region. Interactions between DNA and the amino acid residues of the protein channel have previously been reported to influence blockage current levels in the β-barrel.[40,48] The positively charged Lys and negatively charged Asp residues on the inside wall of the latch region also introduce electrostatic interaction between DNA and the protein wall, which may contribute to the observed sensitivity.[51]

CONCLUSIONS

We have demonstrated an accurate, fast, and label-free method of measuring UDG enzyme activity using the WT α-HL ion channel. The UDG hydrolysis reaction was monitored based on the difference in current blockage levels generated by the reactant and product duplexes captured inside the nanopore. This work can be adapted to monitor the activity of other enzymes that introduce a change in the oligonucleotide structure, and thus provide a new approach for monitoring enzymatic activity on DNA. A potential limitation of this method is that one nanopore might not be able to capture enough events to demonstrate the progress of enzymatic reaction if the reaction is fast and/or the DNA concentration is very low. However, the approach of using nanopore arrays in conjunction with microfluidics can potentially solve the problem, ensuring broader applicability of the nanopore method to monitor a variety of enzymatic reactions.

The ability to distinguish between U and AP is attributed to a recognition site, specific to dsDNA, at the latch entry to the vestibule of WT α-HL. This is in unique contrast to the previously published recognition sites for ssDNA in the central constriction and β-barrel sections of α-HL. We are currently expanding the sensing capability of the latch to other base modification structures, such as mismatch base pairs, single-nucleotide strand breaks, and destabilizing lesions.[52] The discovery of a very sensitive sensing zone at the latch suggests the potential development of new methods to detect site-specific changes in dsDNA structure relevant to epigenetic, forensic, and medical diagnostic applications. Protein mutagenesis that alters the amino acids at the latch region can change the dimension of the channel and the chemical and physical interactions between the channel wall and dsDNA, and is thus potentially useful in the future to enhance the detection sensitivity.

EXPERIMENTAL SECTION

DNA Preparation and Purification Procedures. DNA was prepared from commercially available phosphoramidites (Glen Research, Sterling, VA) by the DNA Core Facility at the University of Utah. Afterward, the DNA was cleaved and deprotected following the manufacturer's protocol, followed by purification using an ion-exchange HPLC column running a linear gradient of B from 25% to 100% over 30 min while monitoring UV absorbance at 260 nm (A = 20 mM NaP_i, 1 M NaCl, pH 7 in 10% CH_3CN/90% ddH_2O, B = 10% CH_3CN/90% ddH_2O, flow rate = 1 mL/min). The AP-containing duplex was prepared by converting U to AP by UDG digestion.

Chemicals and Materials for Nanopore Measurement. A 150 mM KCl, 20 mM Tris·HCl and 1 mM EDTA solution at pH 7.7 was used in both the nanopore and gel electrophoresis experiments. WT α-hemolysin was purchased from List Biological Laboratories in the monomer form of lyophilized powder and dissolved in water at 1 mg/mL. 1,2-Diphytanoyl-*sn*-glycero-3-phospho-choline (DPhPC) was dissolved in decane at 10 mg/mL and used to form the bilayer. Uracil-DNA glycosylase was purchased at 5000 units/mL (New England Biolabs, Ipswich, MA). The bilayer was supported by a glass nanopore membrane (GNM), which was modified with a 2% (v/v) (3-cyanopropyl) dimethylchlorosilane in acetonitrile to create a moderately hydrophobic surface. The DNA duplexes were annealed by mixing the 41-mer and 17-mer at a 1:5 mol ratio, followed by heating in a 90 °C water bath for 5 min and then cooling to room temperature over 3 h.

Current−Time Recordings. Current−time (i−t) recordings were performed at 22 ± 1 °C using a custom-built high-impedance and low-noise system (Electronic BioSciences Inc., San Diego, CA). The KCl solution was used as the electrolyte to fill the solution reservoir and the GNM capillary. A voltage was applied across the GNM between two Ag/AgCl electrodes placed inside and outside of the capillary. A lipid bilayer was deposited across the GNM orifice as indicated by a resistance increase from ∼10 MΩ (associated with the open GNM) to ∼100 GΩ. A pressure of 20 to 40 mmHg was applied to the inside of the GNM capillary using a syringe, allowing the lipid bilayer to be functional for the protein channel reconstitution.[53] Next, 0.2 μL of α-hemolysin monomer solution at 1 mg/mL was added to the *cis* side of GNM (a volume of 350 μL). After protein reconstitution into the lipid bilayer, the duplex DNA (5 nmol at 14 μM for determination of current blockage levels, and 15 nmol at 43 μM for measuring the UDG activity) was added to the solution reservoir. A voltage of −120 mV was applied (Ag/AgCl electrode placed at external solution vs Ag/AgCl electrode inside the capillary). The i−t traces were filtered at 10 kHz and sampled at 50 kHz.

UDG Digestion. In experiments to measure UDG activity, the solution reservoir for nanopore recordings was filled with bovine serum albumin (BSA, New England Biolabs, Ipswich, MA) at 1 mg/mL in 150 mM KCl buffered solution. We found that the enzyme digestion took much longer and the digestion time was not reproducible without the BSA coating. In addition, BSA absorbs on the glass nanopore surface, making the lipid bilayer formed across the nanopore orifice less stable.

The UDG digestion was carried out by adding 20, 28, or 40 pmol of UDG (corresponding to 57, 80.0, or 110 nM in the 350 μL solution

dx.doi.org/10.1021/ja410615d | J. Am. Chem. Soc. 2013, 135, 19347−19353

reservoir) to 15 nmol (43 μM) of duplex starting material in the BSA coated reservoir. The start time, t = 0 min, in monitoring the UDG reaction was set upon the enzyme addition. The concentration of the UDG was determined by the Bradford protein assay as described in SI Figure 4.

Gel electrophoresis analysis for UDG activity was conducted using the same reaction conditions as reported in the nanopore studies. 15 nmol (43 μM) of duplex was treated with 40 pmol (110 μM) of UDG in the 350 μL solution reservoir at 22 ± 1 °C in the 150 mM KCl, 20 mM Tris·HCl, and 1 mM EDTA solution. To conduct the analysis, first the 5′-end of the 41-mer strand was labeled with ^{32}P using [γ-^{32}P]-ATP and T4-polynucleotide kinase (New England Biolabs, Ipswich, MA) following the manufacturer's protocol. Next, the excess [γ-^{32}P]-ATP was removed using a Nap-25 spin-X column (GE Health Sciences). The reaction was doped with ^{32}P-labeled 41-mer to achieve a concentration of 3×10^6 CPM of radiation. Upon commencement of the reaction with the addition of UDG, 2 μL aliquots were removed at 1 min time intervals. Next, the aliquots were added to a 200 mM NaOH solution that was heated at 90 °C for 20 min to quench the reaction and cleave the base-labile abasic sites. The excess salts were removed by dialysis prior to separation of the cleaved strands (product) from the intact strands (reactant) on a 20% polyacrylamide gel that was run at 45 W for 2 h. Reactions were visualized and quantified by storage-phosphor autoradiography on a phosphorimager.

Data Collection. Based on previous reports, i–t blockades that lasted longer than 2 ms were identified as DNA unzipping events.[44] Shorter events were attributed to translocation of excess single-stranded DNA (ssDNA). A 5:1 mol ratio (17-mer versus 41-mer) was used to anneal the DNA, driving the equilibrium between single strands and duplex to the side of duplex formation. The current amplitude of each blockade was used to determine the identity of duplex (AP-or U-containing duplex). Events were extracted using QuB (version 1.5.0.31). Histograms of unzipping durations were plotted using data analysis programs provided by Electronic BioSciences Inc., San Diego, CA. The percentage of AP-containing duplex (i.e., the product of the UDG reaction) was obtained by counting the number of events in the product peak of the current blockade histogram and dividing this to the total number of events for both the product and the reactant in the current blockade histogram.

■ ASSOCIATED CONTENT

Ⓢ Supporting Information

Error analysis, experimental details, and Bradford protein assay. This material is available free of charge via the Internet at http://pubs.acs.org.

■ AUTHOR INFORMATION

Corresponding Authors

*E-mail: burrows@chem.utah.edu.

*E-mail: white@chem.utah.edu.

Notes

The authors declare no competing financial interest.

■ ACKNOWLEDGMENTS

The authors thank Electronic BioSciences Inc. (San Diego, CA) for donating instruments and software, Dr. J. G. Muller (University of Utah) for assistance with mass spectrometry, and Dr. J. M. Harris for discussions regarding data analysis. The work was funded by a grant from the National Institutes of Health (GM093099).

■ REFERENCES

(1) Lindahl, T. *Nature* **1993**, *362*, 709–714.

(2) Frederico, L. A.; Kunkel, T. A.; Shaw, B. R. *Biochemistry* **1990**, *29*, 2532–2537.

(3) Duncan, B. K.; Miller, J. H. *Nature* **1980**, *287*, 560–561.

(4) Imai, K.; Slupphaug, G.; Lee, W.-I.; Revy, P.; Nonoyama, S.; Catalan, N.; Yel, L.; Forveille, M.; Kavli, B.; Krokan, H. E.; Ochs, H. D.; Fischer, A.; Durandy, A. *Nat. Immunol.* **2003**, *4*, 1023–1028.

(5) David, S. S.; Williams, S. D. *Chem. Rev.* **1998**, *98*, 1221–1262.

(6) Lindahl, T. *Proc. Natl. Acad. Sci. U.S.A.* **1974**, *71*, 3649–3653.

(7) Savva, R.; McAuley-Hecht, K.; Brown, T.; Pearl, L. *Nature* **1995**, *373*, 487–493.

(8) David, S. S.; O'Shea, V. L.; Kundu, S. *Nature* **2007**, *447*, 1221–1261.

(9) de Souza-Pinto, N. C.; Harris, C. C.; Bohr, V. A. *Oncogene* **2004**, *23*, 6559–6568.

(10) Neddermann, P.; Jiricny, J. *Proc. Natl. Acad. Sci. U.S.A.* **1994**, *91*, 1642–1646.

(11) Blaisdell, P.; Warner, H. *J. Biol. Chem.* **1983**, *258*, 1603–1609.

(12) Karakaya, A.; Jaruga, P.; Bohr, V. A.; Grollman, A. P.; Dizdaroglu, M. *Nucleic Acids Res.* **1997**, *25*, 474–479.

(13) Dizdaroglu, M.; Bauche, C.; Rodriguez, H.; Laval, J. *Biochemistry* **2000**, *39*, 5586–5592.

(14) Hames, B. D. *Gel Electrophoresis of Proteins: A Practical Approach*; Oxford Univ. Press: Oxford, 1998; Chapter 1.

(15) Kasianowicz, J.; Brandin, E.; Branton, D.; Deamer, D. *Proc. Natl. Acad. Sci. U.S.A.* **1996**, *93*, 13770–13773.

(16) Akeson, M.; Branton, D.; Kasianowicz, J. J.; Brandin, E.; Deamer, D. W. *Biophys. J.* **1999**, *77*, 3227–3233.

(17) Hornblower, B.; Coombs, A.; Whitaker, R. D.; Kolomeisky, A.; Picone, S. J.; Meller, A.; Akeson, M. *Nat. Methods* **2007**, *4*, 315–317.

(18) Lu, S.; Li, W. W.; Rotem, D.; Mikhailova, E.; Bayley, H. *Nat. Chem* **2010**, *2*, 921–928.

(19) Wanunu, M. *Phys. Life Rev.* **2012**, *9*, 125–158.

(20) An, N.; Fleming, A. M.; Burrows, C. J. *J. Am. Chem. Soc.* **2013**, *135*, 8562–8570.

(21) Reiner, J. E.; Balijepalli, A.; Robertson, J. W.; Campbell, J.; Suehle, J.; Kasianowicz, J. J. *Chem. Rev.* **2012**, *112*, 6431–6451.

(22) Robertson, J. W.; Rodrigues, C. G.; Stanford, V. M.; Rubinson, K. A.; Krasilnikov, O. V.; Kasianowicz, J. J. *Proc. Natl. Acad. Sci. U.S.A.* **2007**, *104*, 8207–8211.

(23) Reiner, J. E.; Kasianowicz, J. J.; Nablo, B. J.; Robertson, J. W. *Proc. Natl. Acad. Sci. U.S.A.* **2010**, *107*, 12080–12085.

(24) Balijepalli, A.; Robertson, J. W.; Reiner, J. E.; Kasianowicz, J. J.; Pastor, R. W. *J. Am. Chem. Soc.* **2013**, *135*, 7064–7072.

(25) Payet, L.; Martinho, M.; Pastoriza-Gallego, M.; Betton, J. M.; Auvray, L.; Pelta, J.; Mathé, J. *Anal. Chem.* **2012**, *84*, 4071–4076.

(26) Merstorf, C.; Cressiot, B.; Pastoriza-Gallego, M.; Oukhaled, A.; Betton, J. M.; Auvray, L.; Pelta, J. *ACS Chem. Biol.* **2012**, *7*, 652–658.

(27) Kasianowicz, J. J.; Henrickson, S. E.; Weetall, H. H.; Robertson, B. *Anal. Chem.* **2001**, *73* (10), 2268–2272.

(28) Meller, A.; Nivon, L.; Brandin, E.; Golovchenko, J.; Branton, D. *Proc. Natl. Acad. Sci. U.S.A.* **2000**, *97*, 1079–1084.

(29) Kasianowicz, J. J.; Robertson, J. W. F.; Chan, E. R.; Reiner, J. E.; Stanford, V. M. *Rev. Anal. Chem.* **2008**, *1*, 737–766.

(30) Sauer-Budge, A. F.; Nyamwanda, J. A.; Lubensky, D. K.; Branton, D. *Phys. Rev. Lett.* **2003**, *90*, 238101.

(31) Mathé, J.; Visram, H.; Viasnoff, V.; Rabin, Y.; Meller, A. *Biophys. J.* **2004**, *87*, 3205–3212.

(32) Schibel, A. E. P.; Fleming, A. M.; Jin, Q.; An, N.; Liu, J.; Blakemore, C. P.; White, H. S.; Burrows, C. J. *J. Am. Chem. Soc.* **2011**, *133*, 14778–14784.

(33) Dudko, O. K.; Mathé, J.; Szabo, A.; Meller, A.; Hummer, G. *Biophys. J.* **2007**, *92*, 4188–4195.

(34) Lieberman, K. R.; Dahl, J. M.; Mai, A. H.; Cox, A.; Akeson, M.; Wang, H. *J. Am. Chem. Soc.* **2013**, *135*, 9149–9155.

(35) Benner, S.; Chen, R. J.; Wilson, N. A.; Abu-Shumays, R.; Hurt, N.; Lieberman, K. R.; Deamer, D. W.; Dunbar, W. B.; Akeson, M. *Nat. Nanotechnol.* **2007**, *11*, 718–724.

(36) Cockroft, S. L.; Chu, J.; Amorin, M.; Ghadiri, M. R. *J. Am. Chem. Soc.* **2008**, *130*, 818–820.

(37) Cherf, G. M.; Lieberman, K. R.; Rashid, H.; Lam, C. E.; Karplus, K.; Akeson, M. *Nat. Biotechnol.* **2012**, *30*, 344–348.

(38) Song, L.; Hobaugh, M. R.; Shustak, C.; Cheley, S.; Bayley, H.; Gouaux, J. E. *Science* **1996**, *274*, 1859−1865.
(39) Stoddart, D.; Maglia, G.; Mikhailova, E.; Heron, A. J.; Bayley, H. *Angew. Chem., Int. Ed.* **2009**, *122*, 566−569.
(40) Stoddart, D.; Heron, A. J.; Klingelhoefer, J.; Mikhailova, E.; Maglia, G.; Bayley, H. *Nano Lett.* **2010**, *10*, 3633−3637.
(41) Ashkenasy, N.; Sánchez-Quesada, J.; Bayley, H.; Ghadiri, M. R. *Angew. Chem., Int. Ed.* **2005**, *117*, 1425−1428.
(42) Vercoutere, W. A.; Winters-Hilt, S.; DeGuzman, V. S.; Deamer, D.; Ridino, S. E.; Rodgers, J. T.; Olsen, H. E.; Marziali, A.; Akeson, M. *Nucleic Acids Res.* **2003**, *31*, 1311−1318.
(43) Purnell, R. F.; Schmidt, J. J. *ACS Nano* **2009**, *3*, 2533−2538.
(44) Jin, Q.; Fleming, A. M.; Burrows, C. J.; White, H. S. *J. Am. Chem. Soc.* **2012**, *134*, 11006−11011.
(45) Jiang, Y. L.; Ichikawa, Y.; Song, F.; Stivers, J. T. *Biochemistry* **2003**, *42*, 1922−1929.
(46) Fromme, J. C.; Banerjee, A.; Verdine, G. L. *Curr. Opin. Struct. Biol.* **2004**, *14*, 43−49.
(47) Schibel, A. E. P.; An, N.; Jin, Q.; Fleming, A. M.; Burrows, C. J.; White, H. S. *J. Am. Chem. Soc.* **2010**, *132*, 17992−17995.
(48) Stoddart, D.; Heron, A. J.; Mikhailova, E.; Maglia, G.; Bayley, H. *Proc. Natl. Acad. Sci. U.S.A.* **2009**, *106*, 7702−7707.
(49) Olasagasti, F.; Lieberman, K. R.; Benner, S.; Cherf, G. M.; Dahl, J. M.; Deamer, D. W.; Akeson, M. *Nat. Nanotechnol.* **2010**, *5*, 798−806.
(50) Vercoutere, W.; Winters-Hilt, S.; Olsen, H.; Deamer, D.; Haussler, D.; Akeson, M. *Nat. Biotechnol.* **2001**, *19*, 248−252.
(51) Gu, L. Q.; Dalla Serra, M.; Vincent, J. B.; Vigh, G.; Cheley, S.; Braha, O.; Bayley, H. *Proc. Natl. Acad. Sci. U.S.A.* **2000**, *97*, 3959−3964.
(52) Jin, Q.; Fleming, A. M.; Ding, Y.; Burrows, C. J.; White, H. S. *Biochemistry* **2013**, *52*, 7870−7877.
(53) Schibel, A. E.; Heider, E. C.; Harris, J. M.; White, H. S. *J. Am. Chem. Soc.* **2011**, *133*, 7810−7815.